GMPPT-based PSO-FLC for Solar PV Charging System

Rati Wongsathan*, Isaravuth Seedadan and Kuakoon Intarakamhaeng

Department of Electrical Engineering, Faculty of Engineering and Technology, North-Chiang Mai University, 169 Hang Dong, Chiangmai, 50230 Thailand

rati@northcm.ac.th*(corresponding author), isaravuth@northcm.ac.th and chaiporn089@gmail.com

Abstract. *Solar-powered charging systems have gained increasing attention in various applications. However, ineffective charge regulation can degrade their performance, particularly under partial shading conditions (PSC). To address this problem, a global maximum power point tracking based on particle swarm optimization (GMPPT-PSO) jointly operated with an MPPT-based fuzzy logic controller is proposed. To achieve an optimal charge controller, the main parameters of the GMPPT-PSO are adaptively changed to catch the dynamic PSCs, and all fuzzy parameters are derived and optimized through another PSO to reduce complexity. As a result, the control fuzzy rules have significantly reduced by about 20%. When applied to the battery through constant current-voltage charge, the proposed controller provides a fast transient and reduces the steady-state oscillations that shorten the battery life more efficiently than the conventional controllers. In addition, energy utilization and charging efficiencies, power loss improvement, and charge time reduction are improved by up to 17%, 8%, 20%, and 20%, respectively, over the rest.*

Received by	6 January 2023
Revised by	4 March 2023
Accepted by	28 March 2023

Keywords:

solar charging system, particle swarm optimization, global maximum power point tracking, fuzzy logic controller

1. Introduction

Solar-powered charging systems have increasingly been used to satisfy energy demand in off-grid areas. The maximum solar energy is required to continuously supply the battery to maximize energy utilization while preserving high charging efficiency. In practice, two main techniques used to enable the solar photovoltaic (SPV) generator to operate at the maximum power point (MPP) are the electromechanical-based sun tracker [1] and the power-switching-based MPP tracking (MPPT) [2-6]. The latter is the most used, although their hybridization ensures optimal performance at the cost of increased complexity and expenses [7]. However, achieving accurate MPP tracking is not easily due to the nonlinear and weather-dependent SPV power output characteristics.

In the literature, the conventional MPPT (e.g., proportional-integral-derivative (PID) controller [3]), the hill-climbing algorithms [1-2], and their modified versions have been proposed to apply in the SPV charging system. They are simple and easeful implement but usually detect the MPP in the wrong direction and increase high voltage stress (i.e., spike and oscillations around the MPP), causing heat losses. This problem has been addressed using the additional circuits placed across converter switches [9]. Instead of modifying the converter, the adaptive MPPTs as a soft-switching control, such as neural network-based controller (NNC), and fuzzy logic controller (FLC), provide better control responses and more accurate MPP without oscillations [4-6]. However, over-fitting is the main problem for the NNC. Instead, the MPPT-FLC possessing many control rules is more advantageous. Meanwhile, their hybrids outperform others at the expense of complexity [6]. However, the conventional FLC design may not lead to optimal control.

In the presence of partial shading conditions (PSC), i.e., the non-uniformly distributed solar irradiance over the SPV generator exhibiting multiple-peak of power, mismatch losses drastically decrease the efficiency of the SPV charger-controller. Based on searching a zero gradient of the SPV power-voltage (*P-V*) curves, the above-stated controllers cannot identify the GMPP among the local MPPs. Also, they are frequently stuck on the first local peak, so they fail in tracking GMPP [8]. Alternatively, the GMPPT-based bio-inspired optimizations can overcome such a problem since their searches do not depend on the *P-V* patterns. Several are reported in literature [9-11]. Among them, the PSO, a population-based search with less-used parameters, is the most successfully used. However, the slow rate convergence to the GMPP is a major drawback. In literature, its modifications, such as enhanced leader PSO [10], and FLC-PSO [11], were introduced. Besides, as a time-invariant method, PSO always gets stuck at the first GMPP in the beginning search, which cannot catch the dynamic GMPP under time-varying PSCs.

Herein, this work is to design the GMPPT-PSO assisted with the FLCs for the constant current-voltage (CC-CV) SPV-powered battery charging system. The adaptive-accelerated PSO is used to improve the charging control responses under PSCs. The charger controllers are optimized to increase charging efficiencies while reducing complexity.

2. Method and Methodology

2.1 Description of the Overall SPV Charger-Controller

The SPV charger-controller system (Fig. 1) through the CC-CV (bulk-float) charge consists of four parts: an SPV generator, a buck converter, the battery, and the proposed controller (GMPPT-PSO assisted MPPT-FLC). During CC-charge, if a PSC exists, the GMPPT-PSO searches the GMPP, and the FLC-CC fine-tunes to reduce the power oscillations. An additional PI controller limits the exceeded charge current to prevent overcharge and heat that shortens the battery life. To stabilize the battery voltage when reaching the nominal voltage (14.4 V) and prevent overvoltage, the FLC-CV controls the CV charging to a full charge.

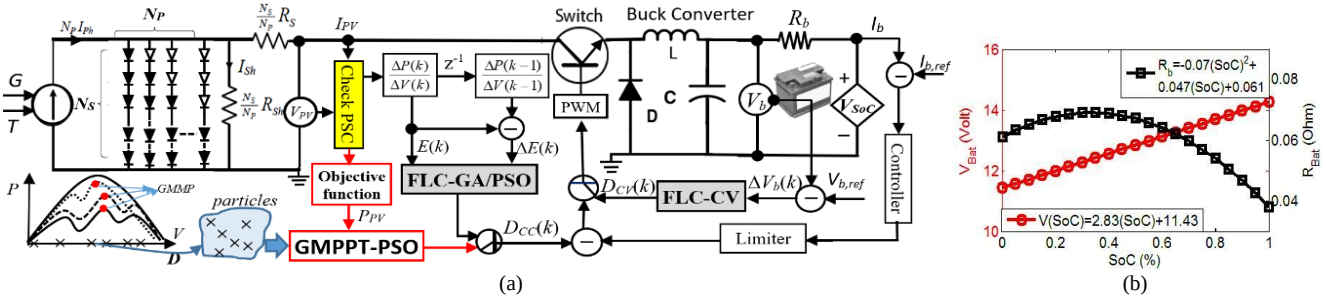

(a) (b)

Fig. 1 (a) Schematic diagram of the proposed SPV-powered battery charger-controller, and (b) The battery voltage and resistance against the SoC.

For the N_S-cell and N_P-string in a series-parallel SPV module (Fig. 1), let $N_{PSC,\,i}$ be the number of shaded cells in the i^{th}-string, and V_{SPV} be the voltage under uniform irradiance. Under PSCs, the voltage of the i^{th}-string of the unshaded cells (N_{UPSC}), $V_{PSC,\,i}$, and the total current (I_{PSC}) related to $V_{PSC,\,i}$ for the given solar irradiance (G) and operated temperature (T) can be respectively expressed by,

$$V_{PSC,i} = N_{UPSC,i} \times V_{SPV} = (N_s - N_{PSC,i}) \times V_{SPV} \tag{1}$$

$$I_{PSC} = \sum_{i=1}^{N_P} \left(I_{ph} - I_{sd} \left[\exp\left(\frac{V^*_{PSC}}{N_{P,i} N_{UPSC,i} V_T} \right) - 1 \right] - \left(\frac{V^*_{PSC}}{N_{UPSC,i} R_{Sh}} \right) \right) \tag{2}$$

where $V^*_{PSC} = N_{P,i} V_{PSC,i} + N_{UPSC,i} I_{PSC,i} R_S$, I_{ph} is the photo-current, I_{sd} is the diode saturation current, R_s is the series resistance, R_{sh} is the parallel resistance, and V_T is the thermal voltage.

Generally, the used SPV module provides more voltage than the battery voltage (V_b). So, the buck converter (Fig. 1) is used to step down V_{PSC} to V_b as in (3) according to a duty ratio (D) generated from the charge controller,

$$V_b = D V_{PSC} \tag{3}$$

In a buck converter design, the interval of D is considered from the SPV and the charging voltage/current ranges. In general, large capacitance and high switching frequency (f_{sw}) are chosen for reducing ripples (γ), but this is an impractical implementation. A more detailed design is referred to in [12].

To deal with lead-acid batteries, the circuit-based model consisting of a controlled voltage source $V(SoC)$ in series with internal resistance $R_b(SoC)$ is used in the simulation (Fig. 1), where SoC is the ratio of the current capacity, in Ah, to the nominal capacity (C). So, V_b can be expressed as,

$$V_b = V(SoC) - I_b R_b(SoC) \tag{4}$$

where I_b is the battery current, $V(SoC)$ and $R_b(SoC)$ can be approximated from the curve-fitted using the experimental data shown in Fig. 1(b), and the updated SoC_t is as follows,

$$SoC_t = SoC_{t-1} + \frac{1}{3600\, fsp} \left(k_b V_b I_b - K_{dc} SoC_{t-1} \right) \tag{5}$$

where K_b is the charging parameter, K_{dc} is the self-discharge rate, and f_{sp} is the sampling frequency.

Using V_b (5) and $R_b(SoC)$ (Fig. 1(b)), the charge efficiency (η_{ch}), as a ratio of total energy stored (E_b), determined by the integral of work done by battery voltage, and an energy loss (E_{loss}) due to the battery resistance during the initial and final SoC [SoC_i, SoC_f], can be obtained by,

$$\eta_{ch} = \frac{E_b}{E_b + E_{loss}} \approx 1 - \frac{C(\Delta SoC)}{\Delta t} \left(\frac{(\Sigma SoC)^2 - (\Lambda SoC) - 2.65}{0.017(\Sigma SoC) + 0.138} \right) \tag{6}$$

where $\Delta SoC \equiv SoC_f - SoC_i$, $\Sigma SoC \equiv SoC_f + SoC_i$, $\Lambda \text{SoC} \equiv \Sigma SoC + SoC_f \times SoC_i$, and Δt is charging time in second.

2.2 The Charger-Controller Design

The operating stepwise of the SPV charger controllers is shown in Fig. 2 (a), which comprises three subroutines: GMPPT-PSO, MPPT-FLC-CC, and FLC-CV.

At the initial stage, 3% of the SPV current at the MPP is set as the threshold (I_{th}) to decide whether the operating point changed. When $\Delta I = I_{PV}(k) - I_{PV}(k-1)$ is more than I_{th} means the weather conditions are changed, so the FLC-CC is activated for tracking a new power ($P_{FLC\text{-}CC}$). Next, if $|P_{FLC\text{-}CC} - P_{max}|$ is higher than the threshold power (ΔP_{th}), as about 5% of P_{max} obtained from Eq. (1) and (2) for $N_{PSC} = 0$, this MPP is assumed to be the local MPP. Then, the GMPPT-PSO is taken-actioned on tracking the GMPP which is further refined by the MPPT-FLC-CC. The FLC-CV finally completes the charge. The details of all subroutines are as follows.

2.3 The GMPPT-PSO

In implementing the PSO for the GMPPT (Fig. 2 (b)), at time k, the duty ratios represented by position vector $\mathbf{D}(k)$=

$[d_1(k), \ldots, d_N(k)]^T$ of the N-particle disperse over the search space [0, 1], and are updated by $\Delta\mathbf{d}$ through the velocity vector $\mathbf{V}(k)=[V_1(k), \ldots, V_N(k)]^T$. In the first step, $\mathbf{D}$ and $\mathbf{V}$ are initiated to regulate the buck converter. The corresponding SPV powers, $\mathbf{P}(k) = [P_1(k), \ldots, P_N(k)]^T$, measured for each particle, are evaluated the strength through the objective function in Eq. (10), but removing the first term of *NR*s, for assigning personnel and global best positions ($\mathbf{P}_{best}(k)$, $G_{best}(k)$). Next, the new velocity $\mathbf{V}(k+1)$, resulting from the vector sum, and the updated $\mathbf{D}(k+1)$ are determined as [13],

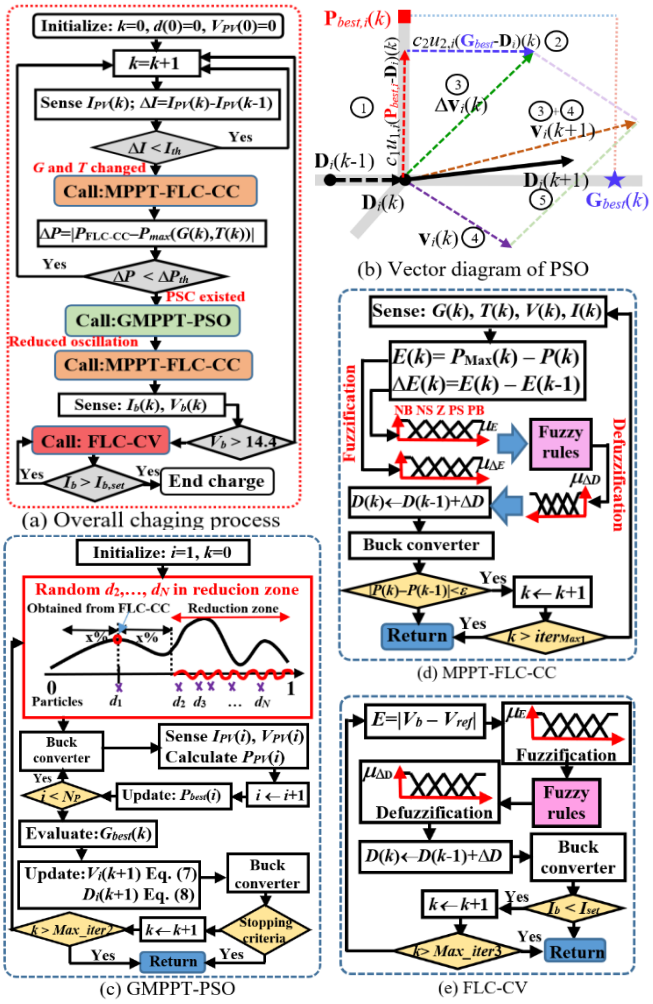

Fig. 2 Block diagram of the SPV-powered charger-controllers.

$$\mathbf{V}(k+1) = \omega\mathbf{V}(k) + c_1u_1(\mathbf{P}_{best} - \mathbf{D})(k) + c_2u_2(G_{best}\mathbf{1}_N - \mathbf{D})(k) \quad (7)$$

and

$$\mathbf{D}(k+1) = \mathbf{D}(k) + \mathbf{V}(k+1), \quad k = 1, 2, \ldots, K \quad (8)$$

respectively, where $\mathbf{1}_N$ is a 1s vector of length N, ω is the inertia constant, c_1 and c_2 are private and social learning rates, u_1 and $u_2 \sim$ N(0, 1), and K is the maximum iteration.

After evaluating the SPV powers for all updated d_i, $\mathbf{P}_{best}$ and G_{best} are updated; $\mathbf{P}_{best,\,i}(k+1) = \mathbf{D}_i(k)$, if $P_i(k) > P_{best,\,i}(k)$ and $G_{best}(k+1) = P_{best,\,i}(k)$, if $P_i(k) > G_{best}(k)$, $i = 1, \ldots, N$. To bound solutions, if $d_i(k) > 1$, $d_i(k) = 0.95$, else if $d_i(k) \le 0$, $d_i(k) = 0.05$. The iteration terminated when met the stopping criteria. In general, the PSO parameters, i.e., ω, c_1, and c_2, are predefined and fixed. For the GMPPT, various methods were applied to parameter selection, e.g., [ee1-2]. However, they are not a generalization. To increase the degree of freedom in optimization and adaptive with the dynamic PSCs, those are included in $\mathbf{D}$ and simultaneously optimized with the duty ratios, where ω, and c_1 and c_2 range in $[\omega_{min}, \omega_{max}]$, and $[c_{min}, c_{max}]$, respectively. Moreover, a technique to reduce the searching region or reduction zone is conducted around the vicinity of the first local peaks obtained from the MPPT-FLC-CC about $|x|$% (in Fig. 2(c)), thus accelerating the convergence of the PSO.

2.4 The MPPT-based FLC-CC optimized by PSO

In the FLC-CC design (Fig. 2(d)), let dP_{SPV}/dV_{SPV} (E) and its change (ΔE) be the fuzzy inputs, and the increment duty ratio (ΔD_{CC}) be the controlled output. Through the three steps based on the Mamdani fuzzy inference system (M-FIS), starting with fuzzification, the crisp of E and ΔE is mapped, respectively, to fuzzy values, $\mu(E)$ and $\mu(\Delta E)$, by five spanning Gaussian membership functions (GMFs) that cover the range of SPV voltage, each including *NB*, *PB*, *NS*, *PS*, and *Z*. Next, the IF-THEN rules evaluate the j^{th}-fuzzy output with the max-min operation, $\mu(\Delta D_{CC,j}) = \max(\min\{\mu(E), \mu(\Delta E)\})$. Finally, ΔD_{CC} is defuzzied by,

$$\Delta D_{CC} = \sum_j \Delta D_{CC,j}\mu(\Delta D_{CC,j}) \Big/ \sum_j \mu(\Delta D_{CC,j}) \quad (9)$$

Here, all fuzzy parameters are offline adjusted by another PSO to obtain the optimal MPPT-FLC. First, M-particle is randomly generated, each possessing vector $\mathbf{F}_{CC}$ containing the GMFs parameters, i.e., mean (c) and deviation (σ) of E, ΔE, and ΔD_{CC}, (2×3×5 parameters) and 5×5 fuzzy rules each represented by 0 or 1, where '0s' and '1s' mean redundant and significant rules, respectively. In training, after the MPPT-FLC took the $\mathbf{F}_{CC}$ into the M-FIS and generated the duty ratio, $D_{CC}(k)=D_{CC}(k-1)+\Delta D_{CC}$, the buck converter is regulated by the PWM signal to move the current operating point ($I_{SPV}(k)$, $V_{SPV}(k)$) to the new one at $k+1$. The transient and steady errors between the power obtained by the MPPT-FLC ($P_{MPPT\text{-}FLC}$) and $P_{MPP(G,\,T)}$ are collected. The strength of the i^{th}-particle at the j^{th}-iteration is evaluated through the following multi-objective function, i.e., minimizing the errors while reducing the redundant rules,

$$fitness_{i,j} = \frac{NR_{i,j}}{NR_{i,j-1}} \times \frac{1}{\sum_{k=1}^{SP}\left|P_{MPP(G,T)} - P_{MPPT-FLC}(i,k)\right|} \quad (10)$$

where *NR* and SP are the number of fuzzy rules and samples.

The performance of the proposed MPPT controller represented by the energy utilization efficiency ($\eta_{utilize}$) over the charging time interval $[t_i, t_f]$ can be expressed as

$$\eta_{utilize} = \int_{t_i}^{t_f}\left(P_{MPPT}(t)/P_{MPP(G,T)}\right)dt\,. \quad (11)$$

2.5 The FLC-CV Optimized by PSO

In the FLC-CV design, let V_b–$V_{b,ref}$ (ΔV_b), and ΔD_{CV} be input and output, respectively. They are fuzzified through 3 spanning GMFs: *NS*, *Z*, and *PS*. So, 6 GMF parameters (3-c's and 3-σ's) are adjusted, and a total of 3 fuzzy rules is not needed to reduce. In M-FIS, the output of the j^{th}-fuzzy rule is $\mu(\Delta D_{CV,j}) = \mu(\Delta V_b)$, where $\mu(\Delta V_b)$ and $\mu(\Delta D_{CV,j})$ are the fuzzy values of ΔV_b and $\Delta D_{CV,j}$, respectively. The crisp output ΔD_{CV} is determined through Eq. (9). For the FLC-CV/PSO, the *Q*-particle each possessing $\mathbf{F}_{CV}$ containing the GMF parameters is taken into the M-FIS. In the beginning, V_b at the last iteration of the CC-charge is taken to compute ΔV_b. After generating the duty ratio, $D_{CV}(k) = D_{CV}(k-1)+\Delta D_{CV}$, to regulate the buck converter, the new $V_b(i, k)$ is measured. Until I_b is less than $I_{b,\,set}$ (1.5 A), the differences between V_b and $V_{b,\,ref}$ are cumulative to determine the strength through,

$$fitness_{i,j} = \sum_k \left(|V_{b,ref} - V_b(i,k)| + 1 \right)^{-1}. \qquad (12)$$

3. Results and Discussion

For modelling the SPV solar battery charging system, all pre-controlled datasets are collected from the experiments (Fig. 3(a)). The commercial 8-cell and 4-string in a series-parallel SPV generator are tested under varying *G* and *T* of uniform irradiance and PSC (Fig. 3(b)) by using the pseudo-solar irradiance. The system parameters used include SPV module; P_{max}(STC) = 130 W, V_{OC} = 22V, I_{SC} = 8.09 A, I_{ph} = 8.01 A, I_S = 8.77 μA, R_s = 0.016 Ω, R_{sh} = 697.7 Ω, buck converter; inductance = 250 μH, capacitance = 20 μF, γ = 5%, f_{sw} = 20 kHz, lead-acid battery; C = 50 Ah, K_{dc} = 0.054, K_b = 0.95, GMPPT-PSO; [ω_{min}, ω_{max}] = [0.2, 1.2], [c_{min}, c_{max}] = [1, 2], N = 5, and FLCs; $E \in$ [-200, 200], $\Delta E \in$ [-100, 100], $\Delta V_b \in$ [-10, 10], $\Delta D \in$ [-2, 2], $M = Q$ = 10. The simulations used the above-said parameters are implemented using MATLAB software.

The proposed PSO converges to the GMPP more efficiently than the conventional PSO (as shown in Fig. 4 (a)), however, both result in oscillations around the GMPP at steady state. For the optimization of FLC-CC and FLC-CV by PSO, the convergence to the best solutions is shown in Fig. 4 (b) and (c). For the FLC-CC, 5 redundant rules are removed from a total 25 rules means reducing 20% complexity. The best shapes of GMFs of FLC-CC and FLC-CV from the PSO are depicted in Fig. 5 (a)-(c), and (d)-(e), respectively.

The charging control results using the proposed controller under PSCs are shown in Fig. 6, which achieves CC-CV charge. It reaches the nominal voltage during the CC charge and regulates near the nominal voltage with about 96% of accuracy during the CV charge. However, their operating points vary depending on the switching regulated by the controlled duty ratios. The transient and steady-state responses of the proposed controller are compared with those of the other charger controllers for some PSCs (Fig. 7).

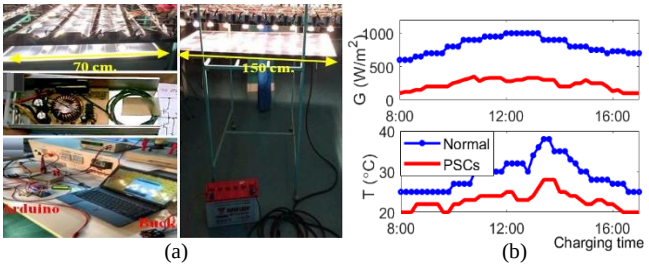

Fig. 3 (a) Hardware settings, and (b) Weather conditions in testing.

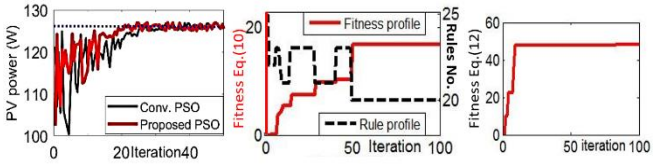

Fig. 4 Convergence of the PSO for the charger-controllers.

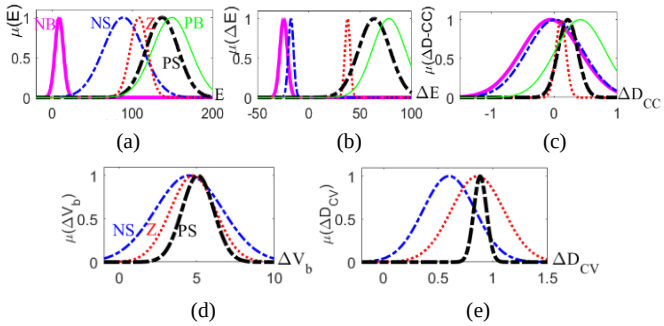

Fig. 5 The best GMFs of MPPT-FLC-CC/PSO for (a) *E*, (b) Δ*E*, and (c) ΔD_{CC} and FLC-CV for (d) ΔV_b, and (e) ΔD_{CV}.

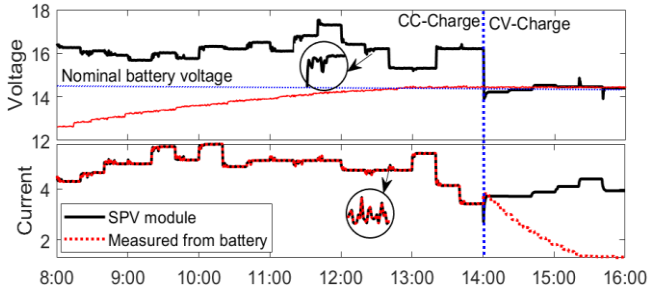

Fig. 6 The charging control results of the proposed charger-controller.

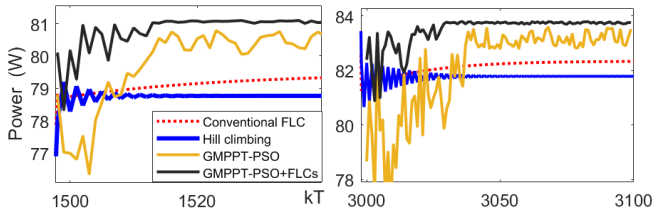

Fig. 7 Transient and steady-state responses under PSCs.

It is seen that the proposed GMPPT-PSO/FLCs controller provides fluctuated powers in the early due to the PSO until reaching the GMPP without oscillations, whereas the GMPPT-PSO results in more oscillations. Besides, the conventional FLC gives a slow transient response with negligible overshoot, nor oscillations, whereas the hill-climbing controller provides a fast response but oscillations.

However, their tracking powers trapped in the local MPP are lower than those of the proposed controllers based on GMPPT, shown in comparison in Fig. 8(a).

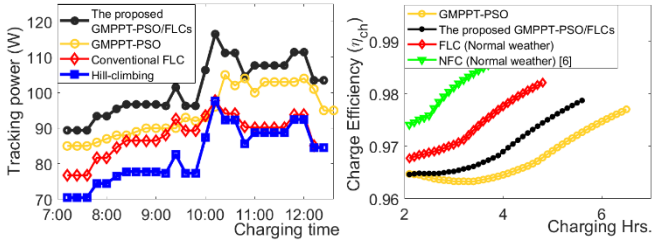

(a) (b)

Fig. 8 A comparison of the charger-controllers' performances of (a) tracking power, and (b) charging efficiency.

The proposed GMPPT-PSO/FLCs, the GMPPT-PSO, the FLC, and the hill-climbing controller give $\eta_{utilize}$, Eq. (11), about 90%, 86%, 77%, and 73%, respectively. For charging efficiency comparison depicted in Fig. 8(b), the range of η_{ch}, Eq. (6), of the PSO-based controllers varies within 96.5%-97.8% under the PSCs, whereas those of the FLC and the neuro-fuzzy controller [6] varies 96.8%-98.2%, and 97.5%-98.7% under the uniform irradiance. As a result, the high initial fluctuations of the PSO-based controllers inducing more heat losses in the battery reduces the η_{ch} while increasing the charging time to full charge in the presence of PSCs. The results of SoC with time confirm this statement (Fig. 9 and Table 1), achieving 80% of maximum SoC (SoC_{max}) as the criterion, the proposed GMPPT-PSO/FLC outperforms the rest for taking less charging time by 0.3–1.5 hours than the others. Moreover, using (6) at this point and SoC_i = 0.1 and computing η_{ch} of the GMPPT-PSO/FLC not slightly different with the NFC [6], GMPPT-PSO, and FLC yield 84.56%, 84.03%, and 76.82%, respectively, where assuming 80% battery efficiency.

The performance metrics of the proposed charger-controller and the others, and their comparison, are summarized in Table 1. Its superior performance is evident. However, other factors, such as the temperature of the battery and the electronic device losses that were not taken into account in the simulations when developing this charger-controller, could cause the theoretical outcomes to differ from those that would be observed in practice.

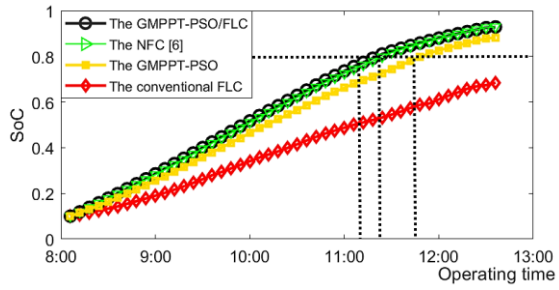

Fig. 9 A comparison of the charging performance in hours per a charge of the charger-controllers under the setting PSCs.

Performance index	Achieving	Percentage improvement
The utilization efficiency ($\eta_{utilize}$)	90%	4%–17%
Nominal power loss	30 W	5% – 20%
The charge efficiency (η_{ch})	84.5%	0.5%–8%
Charging time (hours) per charge	5	5%–20%

Table 1 The performance improvements of the proposed charger-controller compared to the other existing's under the setting PSCs.

4. Conclusion

This study presents the adaptive GMPPT-PSO and the optimal MPPT-FLC to improve charging efficiencies. When applied to the SPV-powered battery charging system through the CC-CV charge under the PSCs, the proposed controller outperforms the others by 4% – 17%, 5% – 20%, 0.5% – 8%, and 5% – 20% for the utilization efficiency, power losses improvement, the charge efficiency, and charging time reduction, respectively. In the future, the microcontroller-based prototype of these controllers will implement for validating the performance of simulations.

Acknowledgements

The research conducted for this paper is sponsored by the Research Institute of North-Chiang Mai University (NCU) and time-supported by the Faculty of Engineering and Technology of NCU.

References

[1] I. Abadi, D. N. Fitriyahah, and A. U. Umam, "Design of maximum power point tracking (MPPT) on two axes solar tracker based on particle swarm fuzzy," *AIP Conference Proceedings*, vol. 2088, no. 1, 2019, pp. 1-11.

[2] N. Tawanna, F. Takkabutr, A. Kesutha, R. Wongsthan, A. Nuangnit, and N. Wongsinlapamorakot, "Improvement performances of PV water pumping system using MPPT-based modified P&O controller: Modeling, setting experimental package and analysis," *The Journal of KMUTNB*, vol. 31, no. 1, pp. 5-15, 2021.

[3] F. A. Mohammed, M. E. Bahgat, S. S. Elmasry, and S. M. Sharaf, "Design of a maximum power point tracking-based PID controller for DC converter of stand-alone PV system," *Journal of Electrical Systems and Information Technology*, vol. 9, pp. 1-15, 2022.

[4] T. Shanthi, "Neural network based MPPT controller for solar PV connected induction motor," *International Journal of Robotics and Automation (IJRA)*, vol. 7, no. 2, pp. 129-139, 2018.

[5] L. K. Narwat and J. Dhillon, "Design and operation of fuzzy logic based MPPT controller under uncertain condition," *Journal of Physics: Conference Series*, vol. 1854, pp. 1-13, 2021.

[6] R. Wongsathan and A. Nuangnit, "Optimal hybrid neuro-fuzzy based controller using MOGA for photo-voltaic (PV) battery charging system," *International Journal of Control, Automation and Systems*, vol. 16, no. 6, pp. 3036-46, 2018.

[7] M. Kamran, M. Mudassar, M. R. Fazal, M. U. Asghar, M. Bilal, and R. Asghar, "Implementation of improved Perturb & Observe MPPT technique with confined search space for standalone photovoltaic system," *Journal of King Saud University – Engineering Sciences*, vol. 32, no. 7, pp. 432-441, 2020.

[8] Y. Shaiek, M. Ben Smida, A. Sakly, M. F. Mimouni, "Comparison between conventional methods and GA approach for maximum power point tracking of shaded solar PV generators," *Solar Energy*, vol. 90, pp. 107-122, 2013.

[9] A. Badis, M. N. Mansouri, and A. Sakly, "PSO and GA-based maximum power point tracking for partially shaded photovoltaic systems," *2016 7th International Renewable Energy Congress (IREC)*, March 22-24, 2016, Hammamet, Tunisia, pp. 1-6, 2016.

[10] P. S. Gavhane, S Krishnamurthy, R. Dixit, J. P. Ram, and N. Rajasekar, "EL-PSO based MPPT for solar PV under partial shaded condition," *Energy Procedia*, vol. 117, pp. 1047-1053, 2017.

[11] C. H. Hussaian Basha and C. Rani, "Performance analysis of MPPT techniques for dynamic irradiation condition of solar PV," *International Journal of Fuzzy System*, vol. 22, no. 5, pp. 1-23, 2020.

[12] A. Wiesner, R. Diez, and G. Perilla, *Design and implementation of a Buck converter with MPPT for battery charge from solar module*, 2013 Workshop on Power Electronics and Power Quality Applications (PEPQA), Bogota, Colombia, July 6-7, 1013, pp. 1-6, 2013.

[13] J. Kennedy and R. Eberhart, *Particle swarm optimization*, Proceedings of ICNN'95 - International Conference on Neural Networks, Perth, WA, Australia, Nov. 27, 1995 – Dec. 1, 1995, pp. 1942-1948 vol.4, 1995.

Biographies

Rati Wongsathan was born in Lamphun, upper northern Thailand. He received his B.Eng. (Hons.) in Electrical Engineering, M. Eng. in Electrical Engineering, M.Sc. in Applied Mathematics from Chiang Mai University (CMU), Chiang Mai, Thailand in 1997, 2000, and 2005, respectively. He completed his PhD in Electrical Engineering from King Mongkut's Institute of Technology Ladkrabang (KMITL), Bangkok, Thailand in 2020. His research interests include renewable energy, mathematical modeling, telecommunications, data storage, optimization, AI, and engineering education. He has published over 30 journal articles with impact factors, 20 conference papers, and 2 books. He currently served as an assistant professor at the Faculty of Engineering and Technology of North-Chiang Mai University (NCU), Chiang Mai, Thailand.

Isaravuth Seedadan was born in Sakon Nakhon, northeastern Thailand. He received his B.Eng. (Hons.) in Electrical Engineering from Vongchavalitkul University, Nakhorn Ratchasima, Thailand in 1992, and M.Eng. in Electrical Engineering from King Mongkut's Institute of Technology Ladkrabang, Bangkok, Thailand in 2003. His research interests include electronic, renewable energy, and engineering education. He currently served as a senior lecturer at Faculty of Engineering and Technology of North-Chiang Mai University (NCU), Chiang Mai, Thailand.

Kuakoon Intarakam-haeng was born in Sukhothai, lower northern Thailand. He is a fourth-year undergraduate student in Electrical Engineering at North-Chiang Mai University, Chiang Mai, Thailand. His research interests lie in the field of digital signal processing. In recognition of his exceptional research work, he was awarded the Best Research Award in Digital Signal Processing at the 45th Electrical Engineering Conference (EECON-45) in 2022.